Acta Cryst. (1979). A**35**, 572–580

High-Resolution Electron Microscopy Images of Defects in Mg- and Li-stabilized β''-aluminas

BY JAN-OLOV BOVIN

Inorganic Chemistry 2, Chemical Centre, University of Lund, PO Box 740, S-220 07 Lund 7, Sweden

(*Received* 10 *October* 1978; *accepted* 29 *January* 1979)

Abstract

Crystals of the magnesium- and lithium-stabilized solid electrolyte β''-alumina have been investigated by high-resolution transmission electron microscopy (HRTEM) and a resolution of 2·7 Å was obtained. Crystals were found to contain two types of defect. Broad close-packed Al—O slabs cause a blockage of the ion-conducting layers in the solid electrolyte. It is shown how such slabs with different widths always have the same type of blocking junction. Growth of the broad Al—O slabs while the ion-conducting layers disappear under the influence of the electron beam was recorded at different stages. The growth always starts in the crystal and moves out to the edge. The broad Al—O slabs grow only to certain thicknesses given by the formula $(4N + 1) \times 2{\cdot}2$ Å. A mechanism for the growth of the broad Al—O slabs is suggested, involving an exodus of $Na + O_2$ or Na_2O followed by a collapse of the conducting layer. The importance of the defects for the understanding of material problems of constructing Na—S batteries with β''-alumina as the solid electrolyte is discussed.

1. Introduction

The highly promising use of Na—S batteries as energy-storage devices is to a great extent dependent on the structural properties of the Mg- or Li-stabilized solid electrolyte β''-alumina. The greatest area of uncertainty with β''-alumina is the nature of certain changes in the material with long-time use, such as loss of sodium ions from the positive electrode side of the electrolyte and changes in structural characteristics (Birk, 1976). The aim of the present investigation was to reveal the nature of the defect structure of β''-alumina by means of high-resolution transmission electron microscopy (HRTEM).

Earlier investigations of β- and β''-alumina by means of transmission electron microscopy have suggested that crystals can contain a number of different types of defects. Thus several authors have suggested that dislocations exist in crystals of β-alumina (Stevens, 1974; LeCars, Gratias, Portier & Théry, 1975; DeJonghe, 1975; Stevens & Miles, 1976; DeJonghe, 1976). Many one-dimensional, low-resolution, 'lattice fringe' pictures have been interpreted in terms of planar (00*l*) intergrowth of β''-alumina and β-alumina (Bevan, Hudson & Moseley, 1974; Gratias, Boilot, LeCars & Théry, 1976). It has been suggested (Sato & Hirotsu, 1976) that the existence of a solubility range for Na^+ in β- and β''-alumina is caused by the possibility of mixed intergrowth of spinel blocks of different width (Bevan, Hudson & Moseley, 1974) between the Na^+-conducting layers; an approach successfully used for barium ferrite compounds (Adelsköld, 1938; Van Landuyt, Amelinckx, Kohn & Eckart, 1974). Later it was shown by DeJonghe (1977*a*), from two-dimensional lattice image pictures, that both stacking-sequence faults and β''-alumina intergrowth in β-alumina crystals could complicate the interpretation of earlier reported images of planar disorder. Structural changes in β-alumina crystals, under the influence of the electron beam, were first reported by Roth (1972) who found that silver whiskers exude from the edge of Ag^+ β-alumina crystals. The existence of dislocations moving through grains of β/β''-alumina have also been proposed (Stevens, 1974). It has been suggested by DeJonghe (1977*b*) that these are due to spinel intergrowth. Blocking defects causing obstacles for Na^+-conduction in β''-alumina has been shown to exist in HRTEM images by Bovin (1978).

Most work before 1977 was performed with electron microscopes possessing limited possibilities of orienting the crystals, which, combined with low resolution, resulted in 'lattice fringe' images showing only one-dimensional (00*l*) resolution. All interpretations of images of β/β''-alumina have so far been made with uncertainty because no comparisons with calculated *n*-beam crystal-structure images have been performed. In the present work the observed and calculated images have been compared. The latter were computed from the atom parameters of β''-alumina (Bettman & Peters, 1969) by use of the multislice method (Cowley & Moodie, 1957; Goodman & Moodie, 1974).

2. The structures of β- and β''-alumina

Both β- and β''-alumina, idealized formulae $Na_2O.11Al_2O_3$ and $Na_2O.5Al_2O_3$, respectively, are

0567-7394/79/040572-15$01.00

hexagonal layered structures. The main feature of the β-alumina structure was determined by Bragg, Gottfried & West (1931) and Beevers & Ross (1937) and refined by Peters, Bettman, Moore & Glick (1971). The unit-cell parameters are $a = 5{\cdot}594$ and $c = 22{\cdot}53$ Å. A natural form of β-alumina is found as the mineral hibonite, $(Ca,Ce)(Al,Ti,Mg)_{12}O_{18}$, with the unit cell, $a = 5{\cdot}61$ and $c = 22{\cdot}16$ Å (Curien, Guillemin, Orcel & Sternberg, 1956). A polyhedral model of the β-alumina structure is shown to the left in Fig. 1. The structure of β''-alumina has been determined by Yamaguchi & Suzuki (1968) from powder data, and from a single crystal of $Na_2MgAl_{10}O_{17}$ by Bettman & Peters (1969). The structures consist of blocks of four layers of cubic close-packed oxygen ions (small colorless balls in the polyhedral models shown in Fig. 1) with appropriate aluminum (in β''-alumina usually also lithium or magnesium) ions in both the octahedral (red and blue in Fig. 1) and the tetrahedral (yellow in Fig. 1) interstices. The cubic close-packed blocks are often referred to as spinel blocks, derived from the similarity of these blocks to the $MgAl_2O_4$ spinel structure (also the same as γ-Al_2O_3). The spinel blocks are held apart by Al—O—Al bridges illustrated by corner-sharing yellow tetrahedra in Fig. 1. The plane of the bridging oxygen ions also contains the sodium ions (or more generally the conducting ion) shown as small blue balls in the models in Fig. 1. The structural relationship between β- and β''-alumina can easily be understood in terms of the crystal-structure building operation, chemical twinning, introduced by Andersson & Hyde (1974). The structure of β''-alumina, here the parent structure, consists of cubic close-packed oxygen ions except in the ion-conducting layers where three-quarters of the oxygen ions are missing. If the chemical twinning operation is applied to the slabs between these layers, *viz* every second red spinel block in the right model of Fig. 1 is rotated π rad around the twin axes (here also the c axis), then the blue slabs in the left model in Fig. 1 are obtained and the β-alumina structure is generated. It has been supposed by Andersson & Hyde (1974) that nature uses the chemical twinning operation to accommodate ions which do not fit the parent structure. From this point of view β-alumina should be the more stable one because it is a chemical twinning of the parent structure β''-alumina with the 'impurity' ion (Na^+) in the twinning plane. The idea is also supported by the fact that other ions like Mg^{2+} and Li^+ are needed to stabilize the structure of β''-alumina. The Mg^{2+} and Li^+ ions are in that case probably situated in the bridging tetrahedra to stabilize the conducting planes.

It is convenient to have a short symbolism to describe the structure of β''-alumina and its defects. Starting the description with the conducting plane of the β''-alumina model (to the right in Fig. 1) it is easily seen that the first layer of polyhedra (on the way up along the c axis) contains only tetrahedra (symbol T), the next layer is just corner- and edge-sharing octahedra (symbol O) followed by a layer of corner- and edge-sharing octahedra and tetrahedra [symbol (OT)]. That completes the three types of layer of polyhedra generating the structure of β''-alumina (also β-alumina). As can be seen in the polyhedron model there are five polyhedron layers $|TO(OT)OT|$ between two conducting layers. β''-alumina can also be described as cubic close-packed as far as oxygen ions are concerned and the packing sequence of oxygen ion layers can thus be written *–abcabca–*. The symbol for an (OT) polyhedron layer between two oxygen layers can for instance be written $-^a(OT)^b-$. The full symbolism of the layer stacking within one unit cell of β''-alumina can thus be written

$$-^a(OT)^bO^cT^aT^bO^c(OT)^aO^bT^cT^aO^b(OT)^cO^aT^bT^cO^a(OT)^b-.$$

The distance between two ion-conducting layers in β''-alumina (twinning planes) is $33{\cdot}85/3 = 11{\cdot}28$ Å. The close-packed oxygen layers above and below the conducting layer are 4·76 Å apart. The approximate distance between two layers within the spinel slab is 2·17 Å.

3. Experimental

(*a*) *Specimen preparation*

Polycrystalline pellets of both lithium- and magnesium-stabilized β''-alumina were prepared. The weights of Na_2O and MgO were 5–6% and 2–4%, respectively, in the samples of magnesium-stabilized β''-alumina and in the case of lithium-stabilized materials 8–10% (Na_2O) and 0·6–0·8% (Li_2O). All samples are in the range commonly used for preparation of sintered tubes for use in Na—S batteries. The pressed pellets of mixtures of high-purity Na_2CO_3, MgO (or Li_2O) and Al_2O_3 were heated in an electrical furnace at 1673–1773 K for 2–5 h in air. All samples were rapidly cooled to room temperature. Preliminary phase identifications were done by means of X-ray powder patterns. In most of the samples both the β- and β''-alumina patterns were seen, with that of β''-alumina predominating. No arrangements were made to prevent possible loss of Na_2O during the preparation.

(*b*) *Electron microscope observation techniques*

Micrographs were taken using a Philips EM 400 electron microscope equipped with a rotation-tilt side-entry goniometer and using an acceleration potential of 120 kV. In order to increase resolution and magnification, the specimen was lifted in the objective lens (Iijima, 1973), giving objective lens current ~5·2 Å instead of ~4·7 Å. The vacuum system of the Philips EM 400 made it possible to study crystals for hours

without any growth of contamination on the surface of the crystal fragments. The time for observation was, in this case, limited by the instability of the β''-alumina structure in the electron beam.

The polycrystalline pellet was ground gently under *n*-butanol in an agate mortar and deposited on a holey carbon film. The samples were not prepared by ion milling in order to be sure of as little influence on the structure as possible. Thin crystal flakes overlapping holes in the carbon film were tilted into the $[10\bar{1}0]$ zone for the recording of micrographs with the 100 μm objective aperture. The 100 μm aperture determines a theoretical resolution of ~1·8 Å and includes approximately 55 beams (*cf.* Fig. 2) which contribute to the image. The shape of the β''-alumina crystals is like mica and only crystals standing on their edge provided the right direction for the $[11\bar{2}0]$ zone which made it very difficult to find suitable crystals. In some aggregates of crystals there were sometimes crystals with the right conditions for observation. All images were recorded using a standard hair-pin filament and an electron optical magnification of ~500 000×. Correction of objective lens astigmatism was carried out at this magnification on the carbon support film by minimizing the contrast.

(*c*) *Calculation of n-beam multislice images*

The physical basis of the multislice method of image calculation was explained by Goodman & Moodie (1974). A computer program, in principle similar to that of Fejes (1973), written by P. Fejes and J. Skarnulis at Arizona State University has been adapted for a Univac 1108 and an Applicon color plotter system using ink jets with a spot size of 0·2 mm at the Computer Center of the University of Lund by C. Svensson and M. Jern.

Through-focus series, from −1000 Å to 600 Å in steps of 100 Å, of images were calculated from the structure parameters of β''-alumina (Bettman & Peters, 1969). The number of slices of the crystals were 3, 5, 7, 9, 13 and 18 with a slice thickness of 5·6 Å. Incident beam convergence used was 7×10^{-4} rad and other values used in the calculations were; spherical aberration constant $c_s = 2{\cdot}5$ mm, focus spread due to chromatic aberration = 100 Å. Several calculations were done for different resolutions (2·0–3·5 Å) and different number of beams (79 and 143) resulting in very little change in the images obtained. Some of the calculated images for 3·5 Å resolution are shown in Fig. 3.

4. Image matching

It has been shown (Cowley & Iijima, 1972; O'Keefe, 1973) that two-dimensional micrographs of thin crystals represent, under proper conditions, the projected potential, or roughly the projected charge density, of the crystal. In the present case of β''-alumina it is necessary for the understanding of the physical properties, to determine the part of the image representing the spinel slabs of the structure and the one showing the conducting layer. Most of the images here presented of β''-alumina crystals are recorded with an underfocus approximately ranging from −400 to −1000 Å, estimated from the behavior of the Fresnel fringe at the crystal edge (Heidenreich, 1964; Bursill & Wilson, 1977). The calculated images covering this range at defocus (*cf.* Fig. 3) with different crystal thickness should be compared with the micrograph in Fig. 2. This micrograph shows a defect-free part of a Mg-stabilized β''-alumina crystal with the best resolution obtained in this investigation. Defocus is estimated to be approximately −700 Å. The upper part of the image can with rather good agreement be compared with the calculated *A–d* (and also with *A–b* and *A–c*) image in Fig. 3. The close relationship shows that the dark fringes of the upper part of the micrograph represent the spinel slabs in the calculated image. The white fringes must consequently represent the conducting layers in β''-alumina. The dark bridges between the dark fringes of the spinel slabs can be interpreted as the Al–O–Al bridges between the spinel slabs (*cf.* Fig. 1) judged from the calculated images. Further down in the micrograph, where the crystal is thicker, two white dots can be seen in the conducting plane between the bridging Al–O–Al. The two dots are first on a horizontal line and then move closer to each other at the same time as the line joining them inclines to the horizontal. The same behavior appears also in the calculated images *B–d* and *C–d* in Fig. 3. The shortest distance between the white dots of the calculated image is $4{\cdot}76/\sqrt{3} \simeq 2{\cdot}75$ Å representing the distance (in projection) between the two empty octahedral positions of the cuboctahedron which can be seen (*cf.* Fig. 1) in the conducting layer. In the micrograph the corresponding distance has been estimated to be approximately 2·7 Å (the distance between the white dots marked with arrows in Fig. 2) showing a remarkably good resolution in just that part of the crystal. In most of the micrographs shown the resolution is however between 3 and 5 Å. It is important to note that for thin crystals, and a defocus of approximately −600 to −1000 Å the dark fringes can be interpreted as spinel slabs and white conducting layers exist between them. How difficult it is to interpret micrographs without a comparison with calculated ones is illustrated by a mistake by DeJonghe (1977*b*), who in a micrograph (*cf.* Fig. 5 in that paper) made the inverse interpretation and in that way wrongly deduced that there was a conducting plane running through the so-called spinel slab of 20·2 Å thickness. For thick crystals (>85 Å) the interpretation is much more complicated (*cf.* Fig. 3).

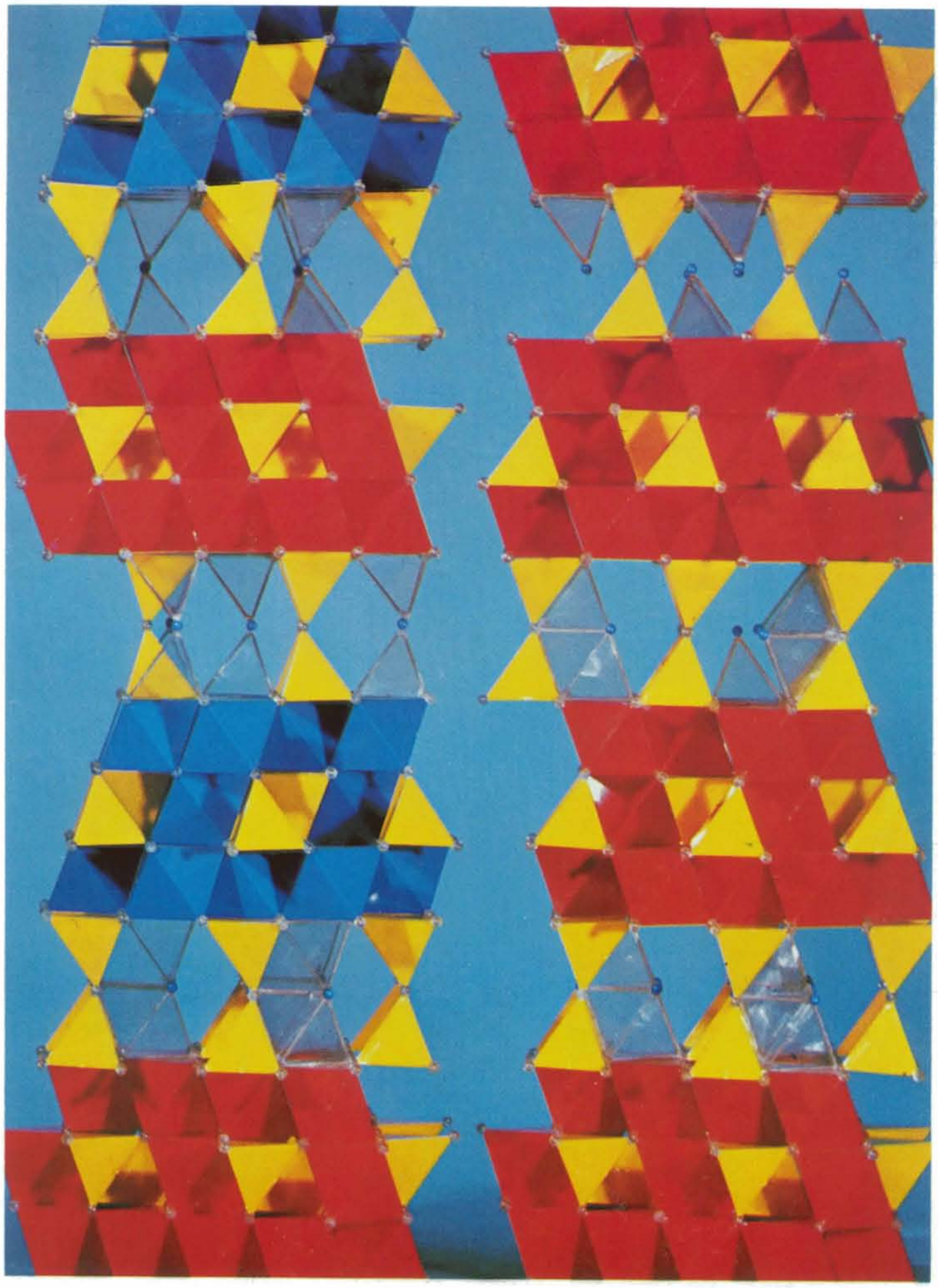

Fig. 1. Polyhedral models of β-alumina (to the left) and β''-alumina structures viewed along the [11$\bar{2}$0] direction. Small colorless balls at the corners of the polyhedra symbolize oxygen ions and small blue ones illustrate the possible positions of the sodium ions in the conducting layers. The red and blue octahedra are centered by aluminum ions and the yellow tetrahedra are centered either by aluminum or in the case of β''-alumina also to some extent by Mg^{2+}/Li^{+} ions.

[*To face p.* 574

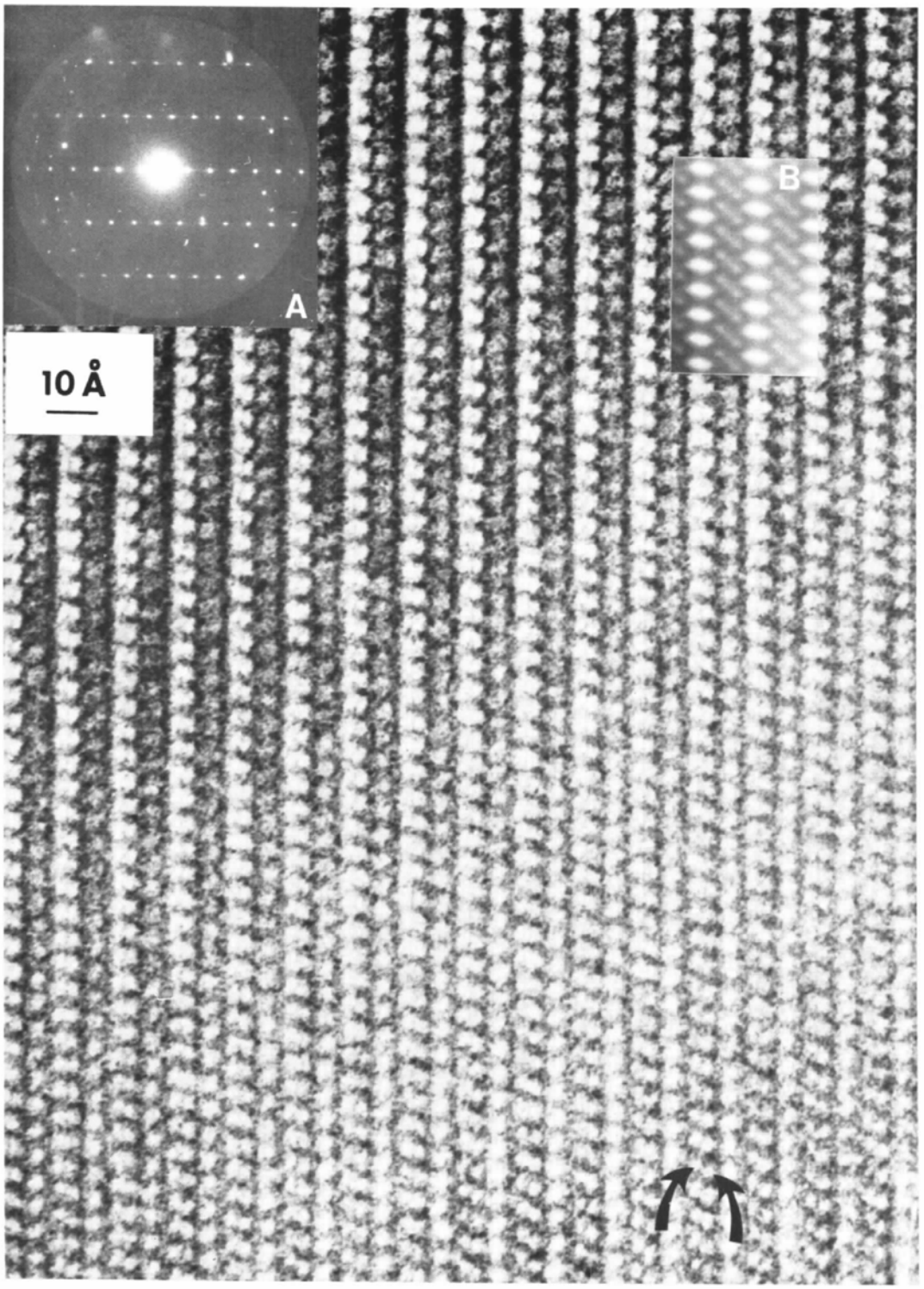

Fig. 2. Micrograph of a thin part of a magnesium-stabilized β''-alumina crystal. The corresponding electron diffraction pattern of the [1120] zone (at *A*) shows the beams within the objective aperture. A computer-simulated image (*A*–*d* in Fig. 3) is inserted at *B*. The resolution of approximately 2·7 Å is marked with two arrows at the bottom of the figure.

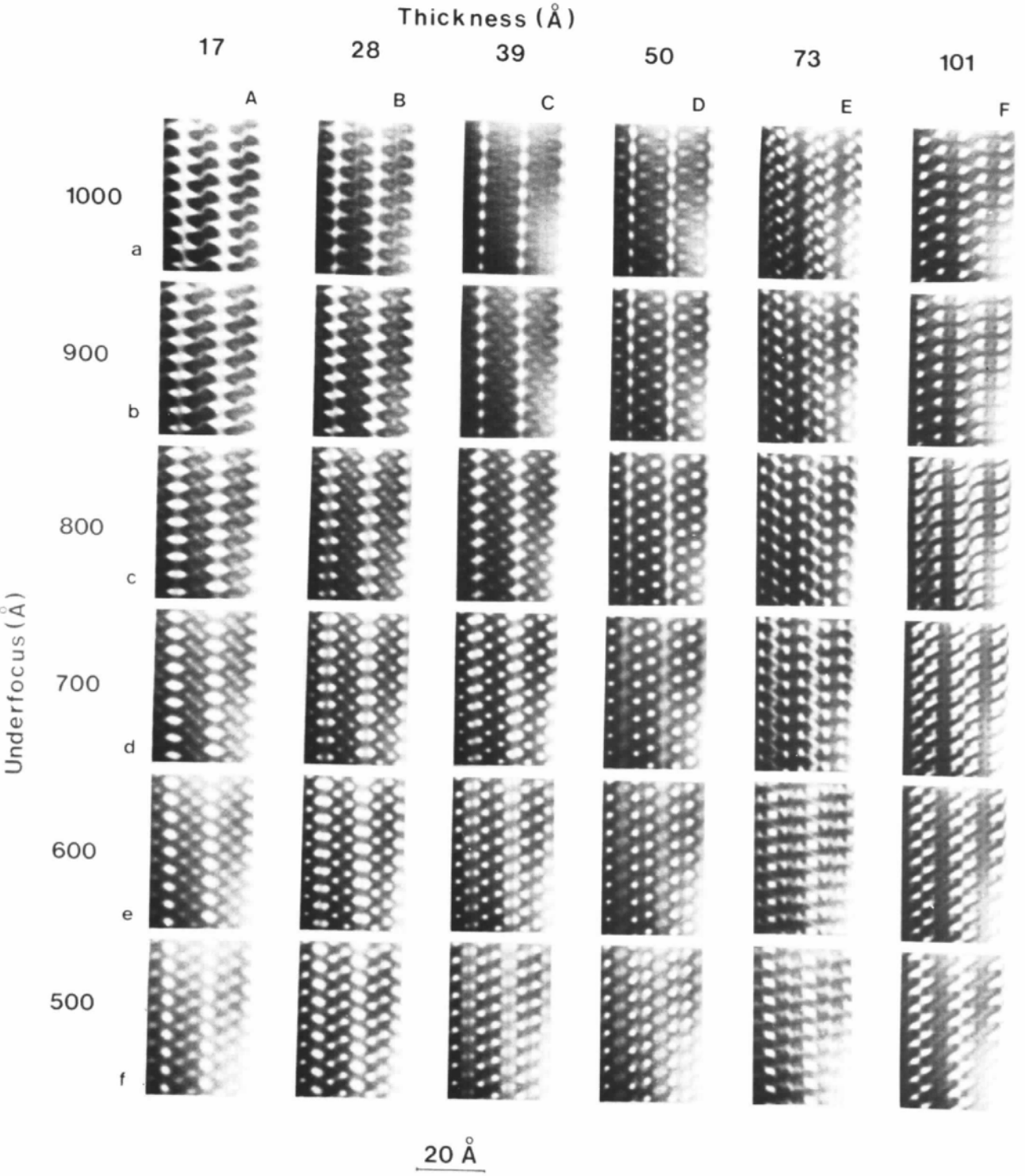

Fig. 3. Through-focus series of calculated n-beam crystal-structure images for the [1120] zone of β'' alumina, $Na_2MgAl_{10}O_{17}$. Origin at the upper left corner.

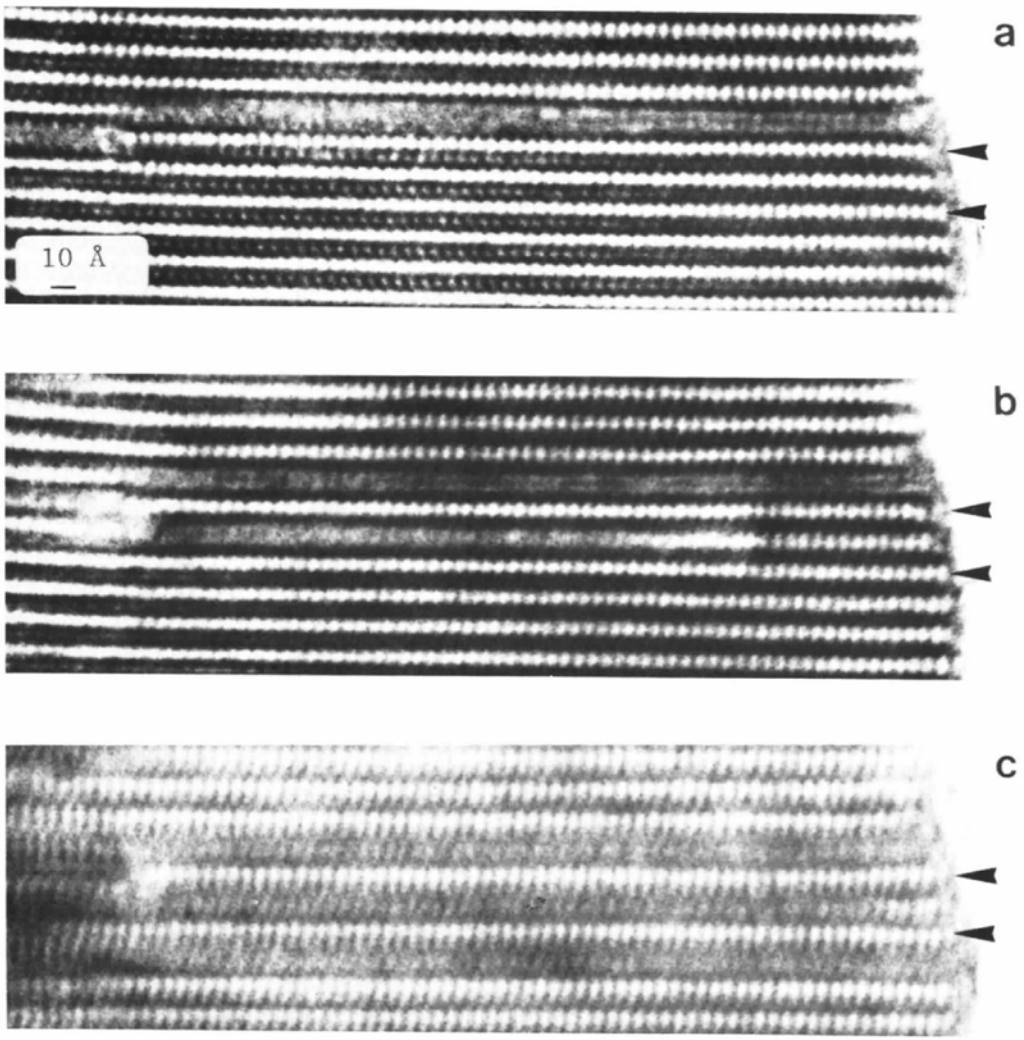

Fig. 5. Three micrographs of the same crystal of magnesium-stabilized β''-alumina obtained with the beam parallel to the [1120] zone showing the effect of the beam irradiation; (*a*) at an initial state and (*b*) and (*c*) recorded after an interval of a few minutes. The broad slab between the two arrows grows from the blocking defect to the left out to the edge of the crystal. A fast-growing broad slab is also turning up in (*c*).

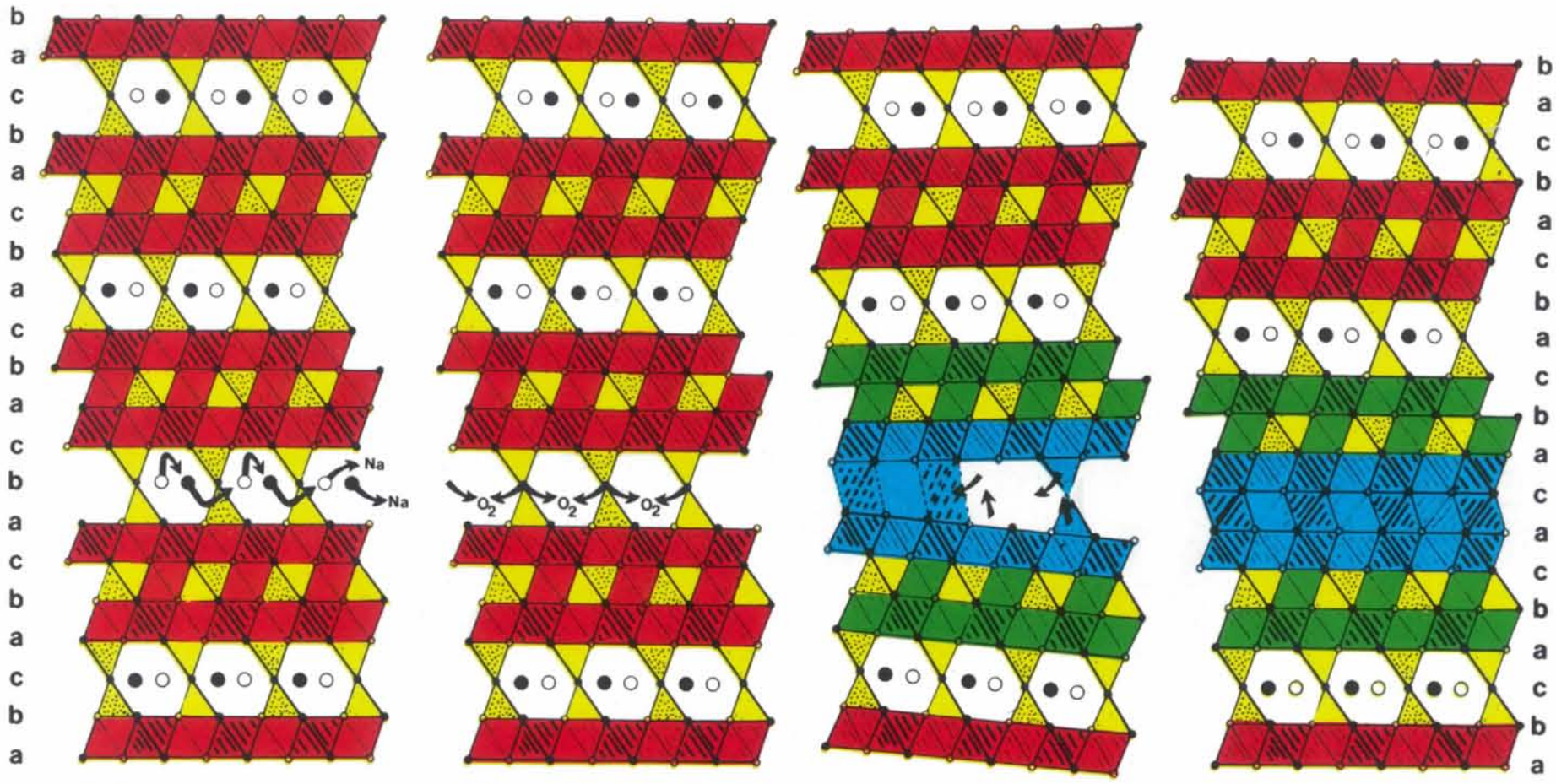

Fig. 8. Drawings of polyhedral models illustrating a possible mechanism for growth of close-packed Al–O slabs. Note that the blue part of the right model has hexagonal close-packed oxygen ions.

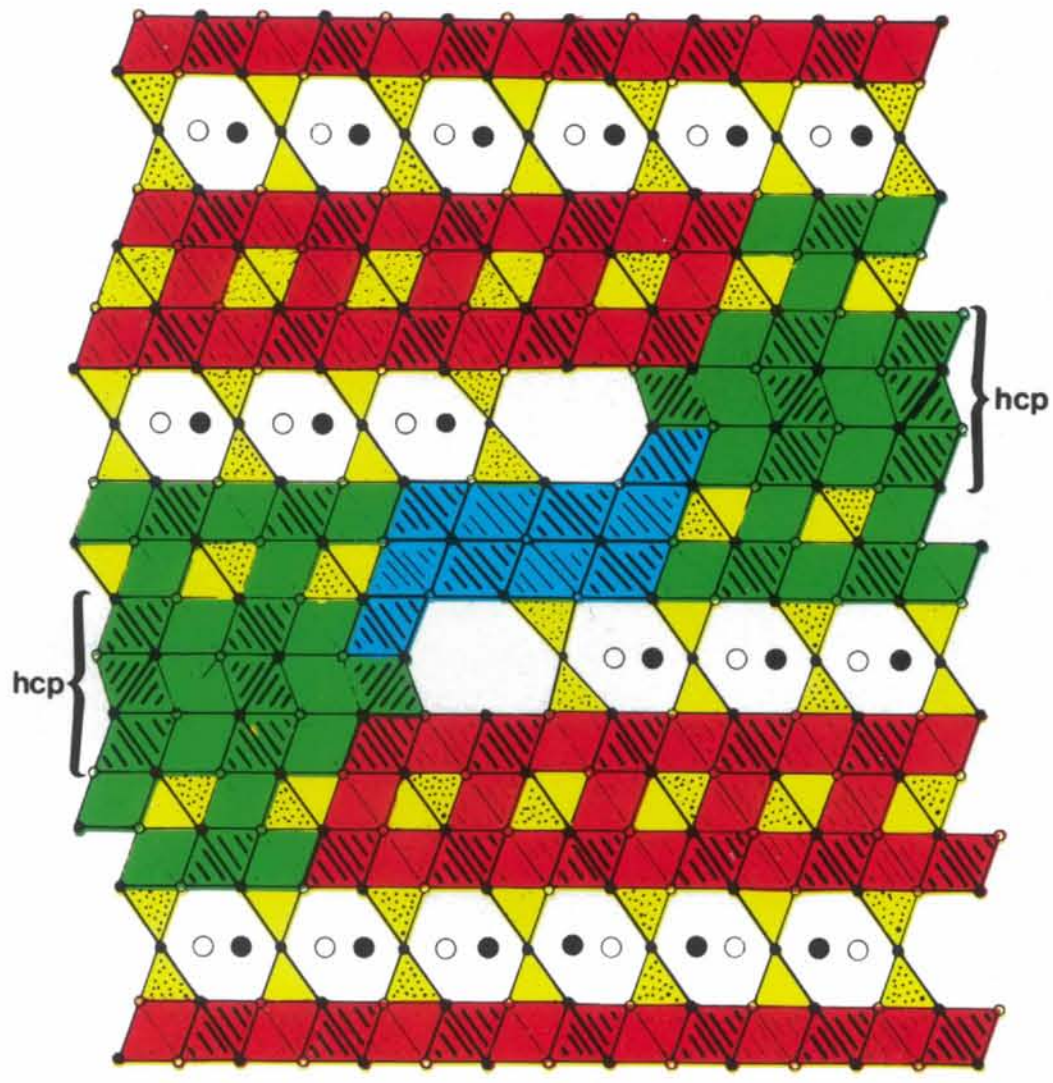

Fig. 11. A drawing of a polyhedron model illustrating a possible structure of the blocking defect in Fig. 4 if the broad slabs are supposed to have a structure generated by the mechanism shown in Fig. 8. The structure is closely related to the one in Fig. 10 with the exception that the octahedra of the junction (blue in the model) are distorted.

5. Structural defects in β''-alumina

All crystals of magnesium- and lithium-stabilized β''-alumina investigated were rich in defects of the kind shown in Fig. 4. The repeat of normal spinel slabs at 11·28 Å, *viz* five layers of polyhedra [–*TO*(*OT*)*OT*–], is interrupted by a 20·3 Å broad slab in the center of the micrograph. This thickness corresponds to nine layers of polyhedra between the conducting layers. Another important type of defect appears to the left of the center of the micrograph. A conducting layer is blocked by the broad slab at the same time as another slab of the same width blocks the succeeding layer. This shows directly how an ionic conducting layer can be blocked by a structural defect in the crystal. The lower part of the micrograph shows two wide slabs. The widest one is 13 layers of polyhedra wide.

(*a*) *The growth of close-packed* Al–O *slabs*

On careful heating of crystals with the electron beam, the images start to change. The most remarkable feature is that some of the ion-conducting layers vanish. It was possible to follow such changes with time, as is illustrated in Fig. 5(*a*), (*b*) and (*c*). The growth of a new close-packed 20·3 Å broad slab (marked with arrows in the figure) starts near a blocking defect and is half the way to the edge in (*b*) and almost finished at the stage shown in (*c*). A fast-growing broad slab, not visible in (*b*), is completed below the first one in (*c*). The disappearance of conducting layers observed in this investigation always starts within the crystal and finishes at the edge. It is worth noting that the distance between the conducting layers at both sides of the created broad slab is not the same before and after change. There is a decrease of approximately 2·2 Å (a fact also registered by DeJonghe, 1977*b*) which is approximately equivalent to the distance between two cubic close-packed oxygen layers in the *c* axis direction. Besides the growth of 20·3 Å broad slabs equivalent to nine layers of polyhedra, there are also ~29·3 Å broad ones. Such broad slabs were created on the disappearance of two conducting layers as can be seen in Fig. 6(*a*), (*b*) and 7(*a*). The distance between the conducting layers at both sides of the slab [marked with arrows in Fig. 6(*a*)] change with an estimated value $(D - D_1)$ of 4·4 Å, indicating that two layers of polyhedra are missing. If all broad close-packed slabs found in crystals of β''-alumina have their origin in disappearing conducting layers there should exist only broad slabs of width $(4N + 1) \times 2{\cdot}2$ Å with the value $N = 1$

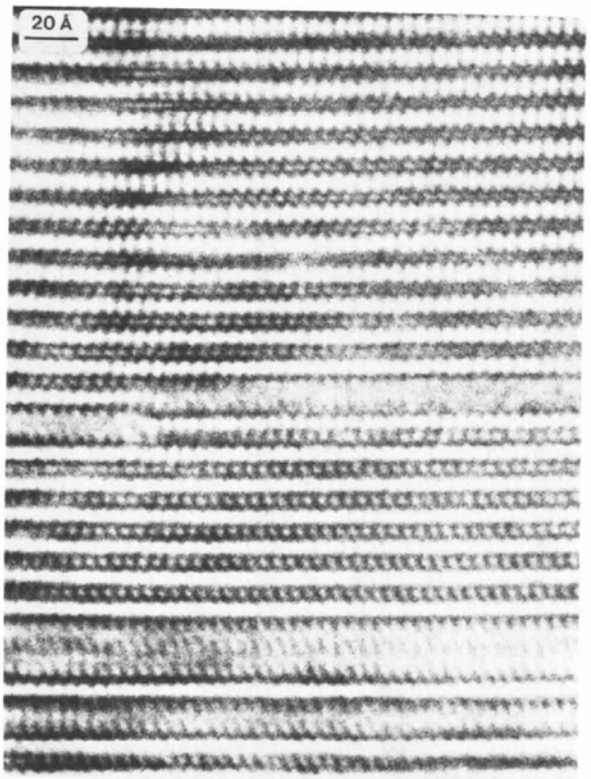

Fig. 4. Crystal-structure image of a magnesium-stabilized β''-alumina crystal. The electron beam is parallel to the [11$\bar{2}$0] zone. The image shows the two types of defects found. Close packed Al–O slabs of different widths sometimes combine to give a defect blocking two conducting layers.

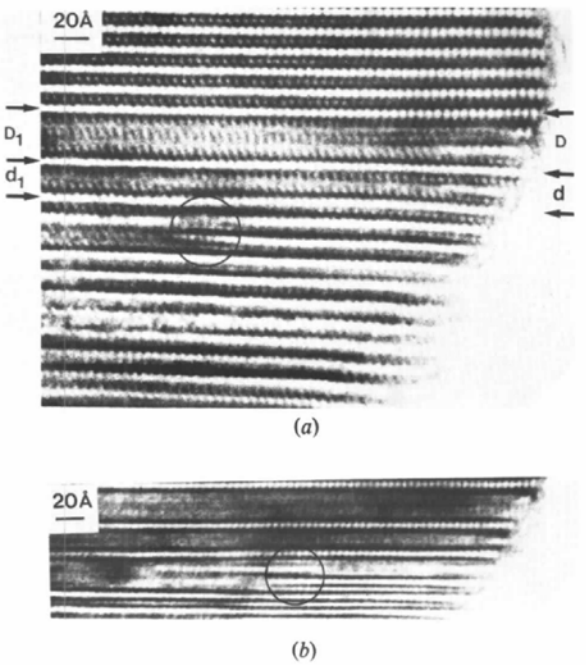

Fig. 6. Two micrographs of the same Mg^{2+}-stabilized β''-alumina crystal taken with an interval of a few minutes. (*a*) and (*b*) illustrate how an ~29·2 Å broad slab grows when two conducting layers disappear. The difference $D - D_1$ is estimated to be 4·4 Å. When one conducting layer vanishes the corresponding difference is $d - d_1$, approximately 2·2 Å. The change generating a blocking defect is illustrated by the area within the circle.

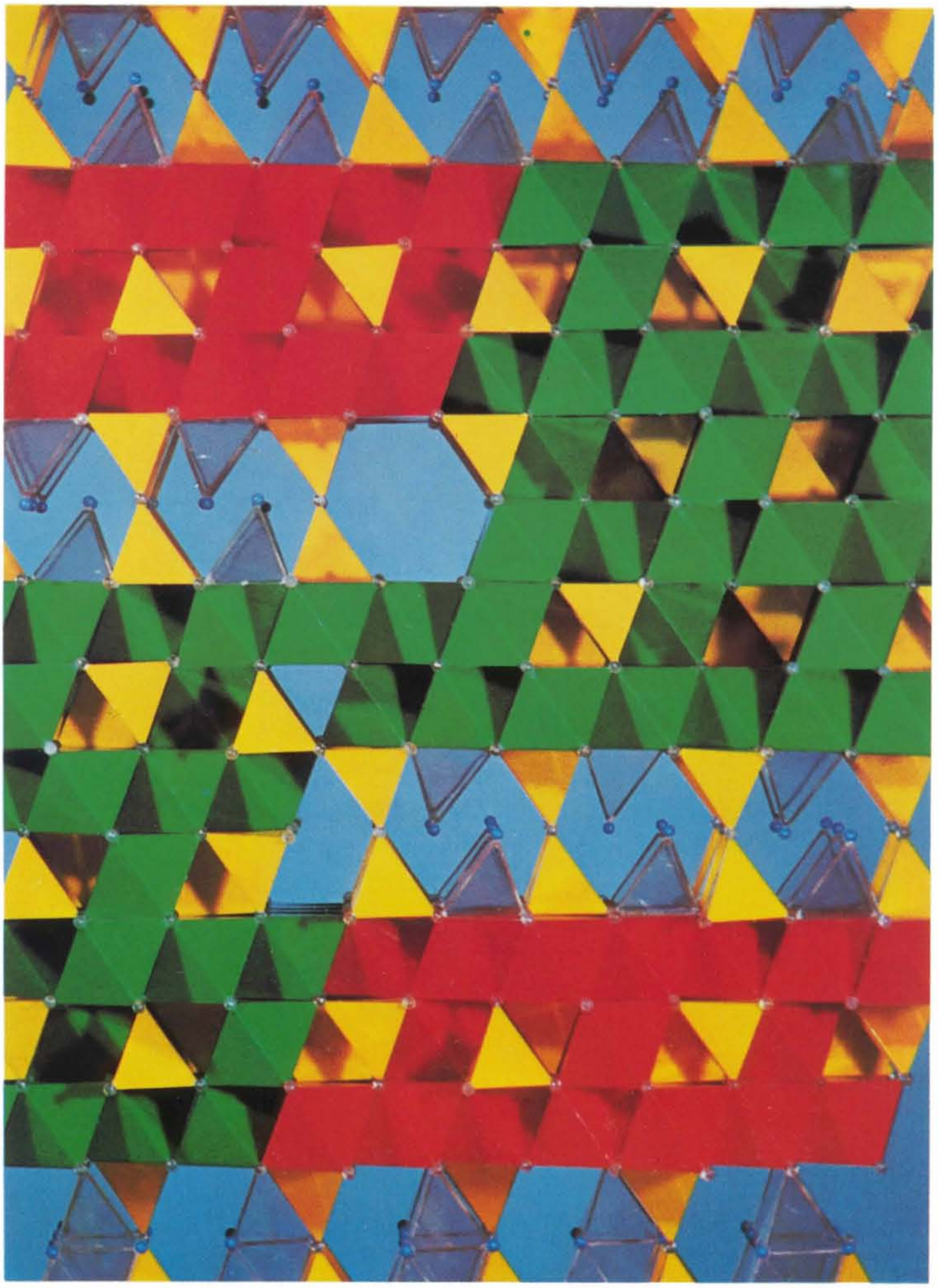

Fig. 10. A polyhedral model showing a possible structure for the blocking defect in Fig. 4 if the broad slabs are supposed to have the spinel structure. The green octahedra are centered by aluminum ions and belong to the nine-layer broad slabs seen in Fig. 4. All other polyhedra and small balls symbolize the same as in Fig. 1.

for normal β''-alumina spinel slabs. This is found to be the case in all β''-alumina crystals here investigated so far. The only broad slabs found contain 9, 13, 17, 21 and 29 layers of polyhedra (*cf.* Fig. 9(*b*), 12 and 14). $4N + 1 = 25$ is probably missing because not enough crystals have been investigated.

The disappearing ion-conducting layer must cause changes in the distances between the oxygen layers of the spinel slabs on both sides. The distance between the two conducting layers above and below the disappearing layer is 22·56 Å, before any change, and after change it is estimated to be 20·3 Å, resulting in a difference of 2·26 Å. But the distance between the conducting layer and nearest oxygen layer (the tetrahedron layer being supposed to vanish) is 2·38 Å. The discrepancy $2{\cdot}38 - 2{\cdot}26 = 0{\cdot}12$ Å must be taken up by changes of the distances of the six ordinary polyhedra layers of the adjacent spinel slabs from 2·17 Å to 2·22 Å in order to generate the 20·3 Å broad slab. The distance 2·22 Å can be compared with the corresponding value of natural spinel; 2·33 Å. The changes of distances (in Å) can be summarized as:

$$\underset{2{\cdot}38}{-T-}\underset{2{\cdot}17}{-O-}\underset{2{\cdot}17}{-OT-}\underset{2{\cdot}17}{-O-}\underset{2{\cdot}38}{-T-}\underset{2{\cdot}38}{-T-}\underset{2{\cdot}17}{-O-}\rightarrow$$

$$\underset{2{\cdot}17}{-OT-}\underset{2{\cdot}17}{-O-}\underset{2{\cdot}38}{-T-}\underset{2{\cdot}38}{-T-}\underset{2{\cdot}22}{-O-}\underset{2{\cdot}22}{-OT-}\underset{2{\cdot}22}{-O-}\rightarrow$$

$$\underset{2{\cdot}22}{-OT-}\underset{2{\cdot}22}{-O-}\underset{2{\cdot}22}{-OT-}\underset{2{\cdot}22}{-O-}\underset{2{\cdot}38}{-T-}\,.$$

It has been suggested (DeJonghe, 1977*b*) that the broad slabs could have spinel structure. If this is the case the stacking order of polyhedron layers from one conducting layer to the one on the other side of the broad slab can be written:

$$-{}^{a}T^{b}O^{c}(OT)^{a}O^{b}(OT)^{c}O^{a}(OT)^{b}O^{c}T^{a}-$$

(see also the right part of the model shown in Fig. 10). The mechanism for the creation of such a nine-layer broad spinel slab can thus be symbolized:

$$-{}^{a}T^{b}O^{c}(OT)^{a}O^{b}T^{c}_{*}T^{a}O^{b}(OT)^{c}O^{a}T^{b}- \rightarrow$$
$$-{}^{a}T^{b}O^{c}(OT)^{a}O^{b}(OT)^{c}O^{a}(OT)^{b}O^{c}T^{a}-$$

where the $-T_{*}T-$ conducting layer transforms to an (OT) layer including an exodus of Na and O_2 (or Na_2O). At the same time the two parts of the crystal have to slip together ~2·2 Å in [33$\bar{6}$4] direction (along one tetrahedron edge). If the (OT) layer of the spinel slab should be generated the mechanism must involve a transport of Al^{3+} ions into the octahedral sites, probably from the surface of the crystal, because the number of ions of tetrahedral coordination in the $-T_{*}T-$ slab is the same as for the (OT) layer. The two conducting layers on both sides of the broad spinel slab are identical as can be seen in the model (*cf.* Fig. 10) and consequently the crystal structure image on both sides should look alike. But this is not in agreement with the crystal structure image shown in Figs. 4 and 5 because the images of the conducting layers are not identical but displaced by $\frac{1}{3}$ of 4·8 Å.

Another possible mechanism for the disappearance of the conducting layer is illustrated in Fig. 8. The structural change is assumed to start with an exodus of sodium caused by the electron beam, a phenomenon known from Ag^{+} β-alumina crystals (Roth, 1972). The oxygen layer *b* in Fig. 8 will thus be very unstable and

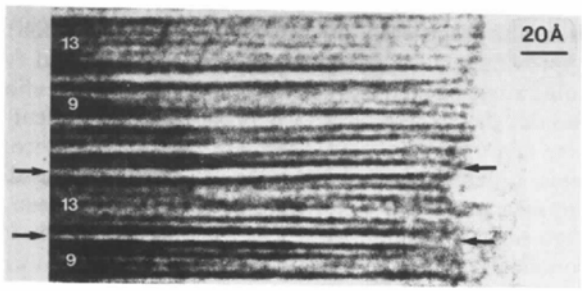

(*a*)

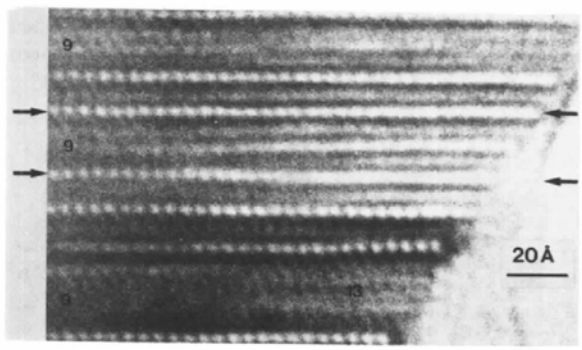

(*b*)

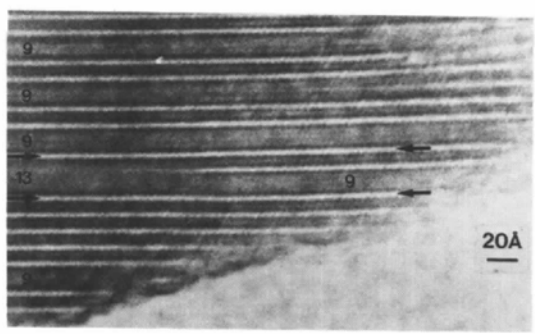

(*c*)

Fig. 7. Three [11$\bar{2}$0] micrographs of Mg^{2+}- (*a*) and Li^{+}- (*b* and *c*) stabilized β''-alumina crystals illustrating that the defect caused by disappearing conducting layers is common. The figures between the conducting layers indicate the number of polyhedra layers in the close-packed slabs. Normal spinel slabs in the β- and β''-alumina structure (*cf.* Fig. 1) of five layers are not marked. In (*a*) two conducting layers disappear and in (*b*) one disappears. One conducting layer disappears in a crystal, shown in (*c*), generating a slab 13 layers broad when a nine-layer broad slab grows together with a normal five-layer spinel slab.

probably collapse under loss of O_2. It is of course also possible that sodium ions react at once with the oxygen ions and Na_2O leaves the conducting layer. But it is worth noting that the sodium and oxygen content of the conducting layer is different from the stoichiometry of Na_2O. In Fig. 5(*b*) can be seen how the part of the disappearing conducting layer which is close to the already close-packed slab is white, indicating that the Al–O–Al bridges vanish before the collapse. The image thus supports the hypothesis above. The two parts of the crystals on both sides of the layer will of course aspire to move closer together and if the adjacent conducting layers on both sides of the defect should be displaced by $\frac{1}{3}$ of 4·8 Å they would have to move together approximately 2·2 Å in the [0001] direction. At the same time, the Al^{3+} ions of the vanishing tetrahedral sites would probably have to move into the octahedral sites as shown in Fig. 8. The [0001] slip generates a three-layer broad slab of octahedra, the blue $-{}^cO^aO^cO^a-$ slab, containing hexagonally close-packed oxygen ions. The blue octahedra share faces like the octahedra in the corundum structure (Al_2O_3). The mechanism can be symbolized:

$$-{}^aO^bT^cT^aO^b(OT)^cO^aT^bT^cO^a(OT)^bO^cT^aT^bO^c(OT)^aO^bT^cT^aO^b- \rightarrow$$

$$-{}^aO^bT^cT^aO^b(OT)^cO^aO^cO^a(OT)^bO^cT^aT^bO^c(OT)^aO^bT^cT^aO^b-.$$

The conducting layer *c* in the final model is equivalent to the next nearest conducting layer above the broad slab and this is in accordance with the crystal structure image in Fig. 5.

It is not possible to determine the structure of the close-packed slabs from the micrographs because it requires a much better resolution (<2 Å) of the electron microscope. But in two crystals it was possible to see an image repeat within the slab. In the micrograph of Fig. 9(*a*), the two-dimensional image repeat along the directions shown in the figure is estimated to be 4·8 Å with an angle $\beta \simeq 71°$. The one-dimensional image repeat along the *c* axis in the crystal shown in Fig. 8(*b*) is also estimated to be 4·8 Å. The expected image repeat corresponding to the [10$\bar{1}$0] zone of β''-alumina should be, for spinel slabs, $\simeq 4{\cdot}8$ Å in both directions with an angle of $\arctan(2\sqrt{2}) \simeq 70{\cdot}5°$. In the case of the second mechanism suggested (*cf.* Fig. 8) with face-sharing octahedra, the corresponding values should show almost the same repeat (the difference should not be possible to estimate in the micrograph) but there should be a slight displacement of the row of white dots. The difference is probably too small to be seen in the diffuse micrograph. The two-dimensional image repeat of the crystal in Fig. 9(*a*) has too poor a resolution for determining the right mechanism.

(*b*) *Blocking defects*

The type of blocking defect seen in Fig. 4 was very frequently found in crystals of β''-alumina. Such a defect will here simply be symbolized by means of the number of polyhedra layers at both sides of the defect junction as $T_l/B_l \sim T_r/B_r$. Where *T* and *B* stand for the number of layers at the top and bottom, respectively, and *l* and *r* stand for left and right side of the junction. The blocking defect shown in Fig. 4 can thus be written $\frac{5}{8} \sim \frac{8}{5}$.

It is always very useful to have the possibility of describing a structure by means of a polyhedral model; in Fig. 10 a possible explanation of the structure of the blocking defect in Fig. 4 is shown by such a model. It is of course impossible to deduce an exact model of the defect from the micrograph because it would require a much better resolution. The polyhedral model shown in Fig. 10 has been built with the intention to get an answer to the following question. What will the junction look like when two nine-layer broad spinel slabs (marked as green octahedra in Fig. 10) bump into each other? It turned out that in the whole polyhedral model of the blocking defect there is just a small area, in the center of the model, where there is a break (deviation from the Al/O ratio of 1·5 in spinel) in the 'normal' β''-alumina packing of octahedra and tetrahedra, because in the center of the model a part of the rocksalt structure (ratio 1) type can be assumed to exist. MgO crystallizes with the rocksalt structure and one possibility is that, at least in the case of magnesium-stabilized β''-alumina, some Mg^{2+} ions can be accommodated in the blocking defect junction when broad spinel slabs run into each other. But, on the other hand, the same defect is seen in lithium-stabilized β''-alumina crystals and Li_2O does not have the rocksalt structure. One detail of the defect in the micrograph was not taken into account when the model was built, namely that the faces of the two conducting layers bend upwards and downwards a little when they run into the broad spinel slabs.

If the close-packed broad slabs are built according to the mechanism illustrated in Fig. 8 the blocking defect will look like the model shown in Fig. 11. In this case the partly h.c.p. slabs (green in the figure) will run into each other resulting in a similar junction compared with the spinel case but here the octahedra (blue in the model) are somewhat distorted.

Blocking defects in other crystals were found to be caused by broad slabs of different widths. The symbolism for those defects found can be written $\frac{9}{9} \sim \frac{13}{5}$ [*cf.* Fig. 12(*a*) and the inverse in 12(*b*); Fig. 13 and Fig. 14(*a*)], $\frac{9}{13} \sim \frac{13}{9}$ [*cf.* Fig. 12(*c*) and Fig. 14(*a*)], $\frac{17}{5} \sim \frac{13}{9}$ [*cf.* Fig. 14(*a*)] and $\frac{13}{13} \sim \frac{9}{17}$ [*cf.* Fig. 12(*d*)]. It is worth noting that in all blocking defects observed, the difference $|T_l - T_r| = 4$ (and consequently $|B_l - B_r| = 4$) corresponding to a distance of approximately 8·8 Å between the planes of the two conducting layers (*cf.* the models in Figs. 10 and 11).

It is not necessary that the junction of the blockade grows parallel to the [11$\bar{2}$0] zone of projection. This

can be seen in the micrographs of Figs. 12 and 14; two conducting layers pass each other and then fade out after passing. For example, the junction can be parallel to the $[10\bar{1}0]$ zone as can be seen in the center of the micrograph of Fig. 13. The crystal has in that case been tilted into this zone, as can be judged by the corresponding electron-diffraction pattern, and the blocking broad slabs end abruptly just where they meet each other.

The question of whether the blocking defect is common in crystals of β''-alumina arises. It can never be answered by means of the electron microscope in reasonable time but the problem can be compared with the classic problem of finding a needle in a haystack. It is most unlikely that the 'needle' can be found many

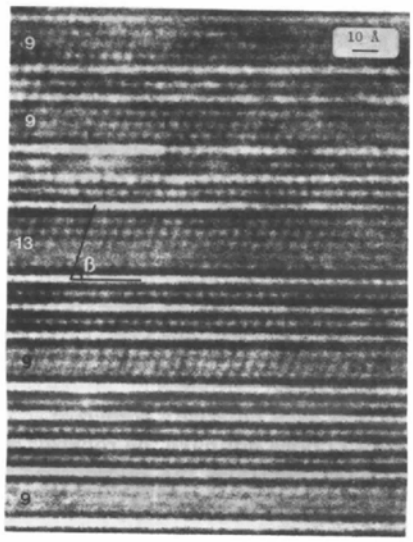

(*a*)

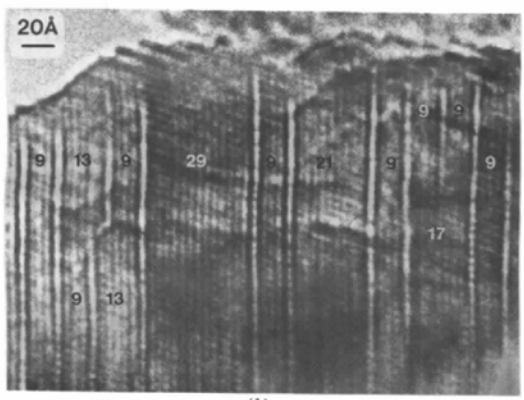

(*b*)

Fig. 9. Two $[11\bar{2}0]$ micrographs of Li- and Mg-stabilized β''-alumina (*a* and *b*, respectively) showing the periodicity of the lattice within the broad close-packed slabs. The angle β in (*a*) is estimated to be 71° and the periodicity of the lattice is estimated to be 4·8 Å in (*a*) and 4·8 Å in the *c* axis direction in (*b*).

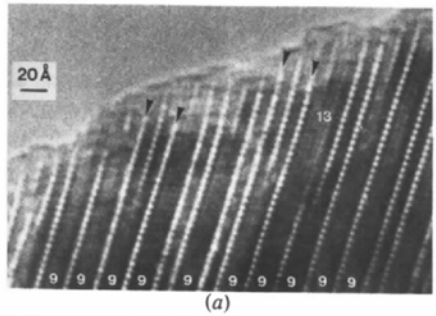

(*a*)

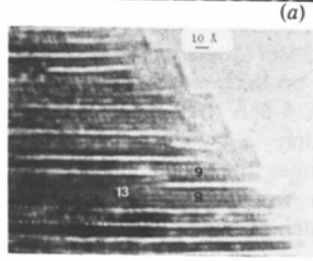

(*b*)

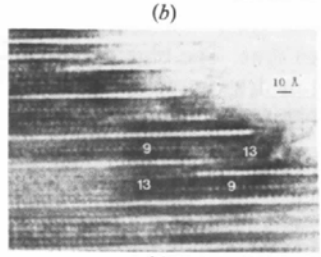

(*c*)

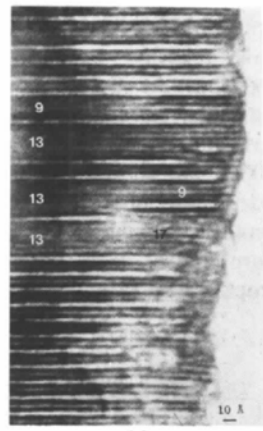

(*d*)

Fig. 12. Four $[11\bar{2}0]$ micrographs showing some of the blocking defects found in Li^+-stabilized β''-alumina crystals. In (*a*) two disappearing conducting layers, generating two nine-layer broad slabs (between the arrows) can be seen.

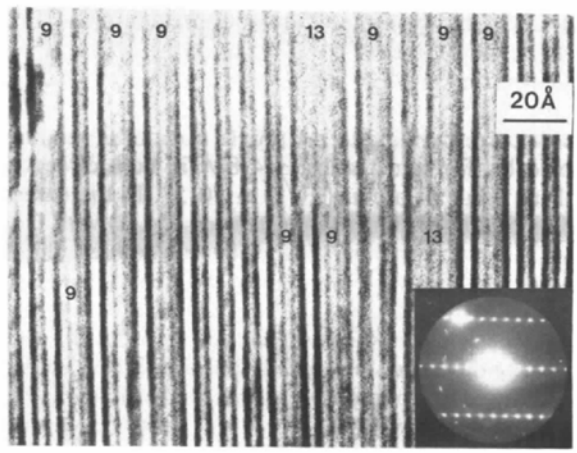

Fig. 13. A $[10\bar{1}0]$ micrograph of a thin Mg^{2+}-stabilized β''-alumina crystal showing broad slabs and a blocking defect. The corresponding electron diffraction pattern shows the beam within the objective aperture.

times in the same 'haystack'. That the two types of defects here discussed are common becomes plausible when one looks at the image of the crystal shown in Fig. 14. The corresponding diffraction pattern also shows how distorted the crystal is in the *c* axis direction but is still in good order in the perpendicular direction.

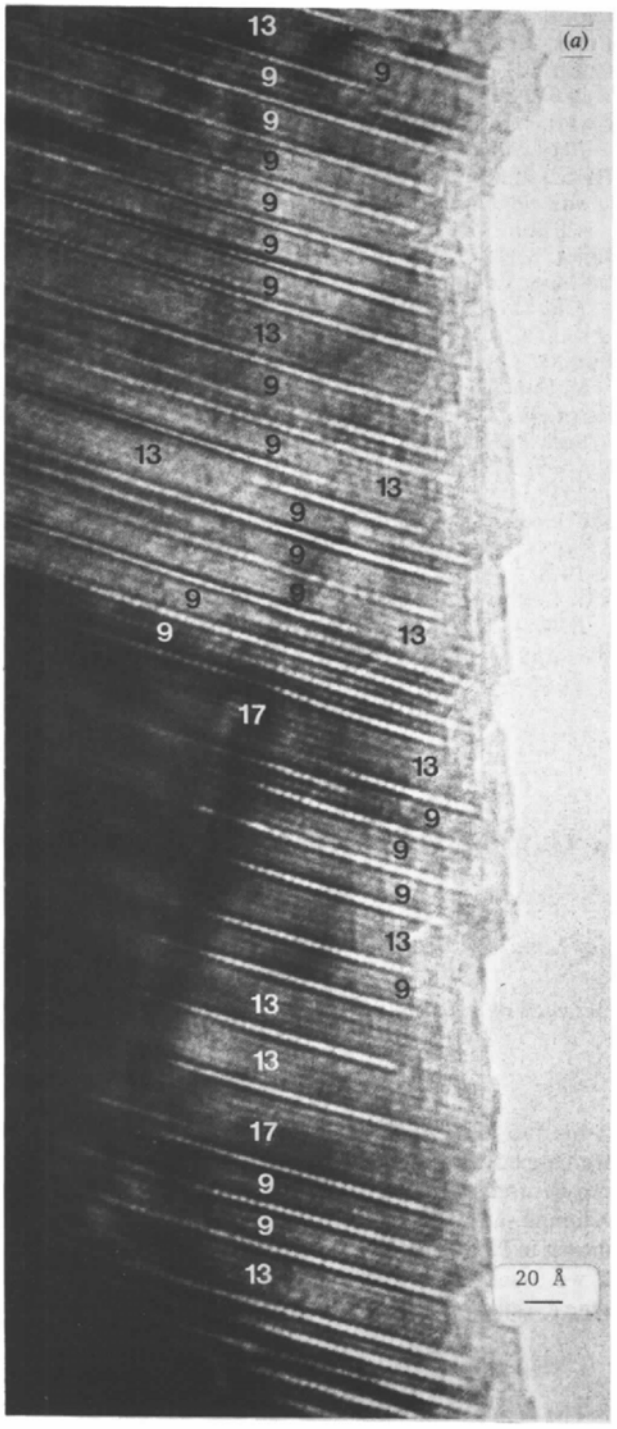

Fig. 14. (*a*) Crystal structure image of a very disordered Li^+-stabilized β''-alumina crystal.

6. Discussion

The defects presented here must affect the ionic conductivity properties of β''-alumina. Blocking defects like those in Fig. 4 will of course reduce the ionic conductivity of the crystal locally. If such defects grow to the extent shown in the crystal of Fig. 14 the changes in properties must be measurable. The serious defect with which battery construction is concerned must be the growth of broad non-conducting Al–O slabs. One can argue that the conditions of the high-vacuum system of the electron microscope cannot be compared with the conditions of the Na–S battery. In most senses that is true, but the ion transport is comparable because in both cases the Na^+ ion is obviously transported out of the conducting layers. In the microscope the Na^+ ions are influenced by the high-energy electrons and move out of the conducting layer either as Na or Na_2O. In the battery the Na^+ ions are transported through the conducting layer, under the influence of the outer electrical field gradient, to react with the liquid sulphur. At the battery working temperature (>573 K) motion of Al^{3+}, Mg^{2+} (or Li^+) and O^{2-} ions giving larger close-packed Al–O slabs competes with an equivalent amount of liquid sodium transformed to Na^+ moving through the solid electrolyte to fill up the conducting layers continuously. If a blocking defect like that in Fig. 5 prevents such a Na^+ ion transport, more broad non-conducting slabs can be produced. If an assumed electrical field gradient, such as occurs in a battery, were parallel with the fringes of the crystal shown in Fig. 5 the mechanism of growth should be the same as found in the microscope, *viz* the growth of broad non-conducting slabs starts within the crystal and ends at the edge. It is obvious that the material gradually loses its conductivity when the non-conducting broad slabs

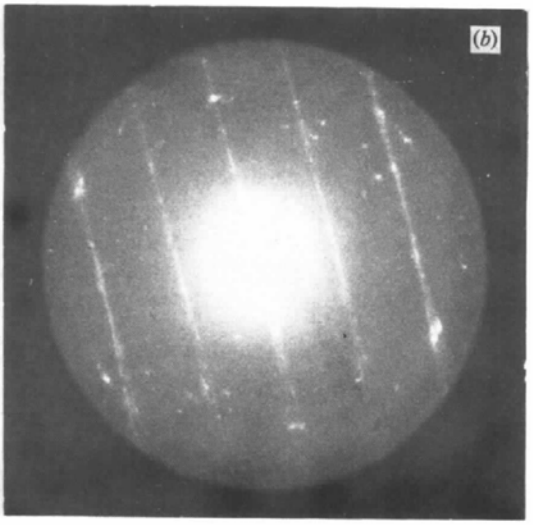

Fig. 14. (*b*) The corresponding electron diffraction pattern of Fig. 14(*a*) shows the streaks parallel to the *c* axis.

cause a decrease in the Na^+ ion concentration close to the liquid sulphur, which also agrees with earlier reported observation (Birk, 1976).

The investigation of β''-alumina by high-resolution transmission electron microscopy will continue in our laboratory and will include material used for extended periods in battery systems.

This work was supported by the Swedish Natural Science Research Council.

References

ADELSKÖLD, V. (1938). *Ark. Kemi Mineral. Geol.* **12A** (No. 29), 1–9.

ANDERSSON, S. & HYDE, B. (1974). *J. Solid State Chem.* **9**, 92–101.

BEEVERS, C. A. & ROSS, M. A. S. (1937). *Z. Kristallogr.* **97**, 59–66.

BETTMAN, M. & PETERS, K. R. (1969). *J. Phys. Chem.* **73**, 1774–1780.

BEVAN, D. J. M., HUDSON, B. & MOSELEY, P. T. (1974). *Mater. Res. Bull.* **9**, 1073–1084.

BIRK, J. R. (1976). *Proc. Conf. Superionics on Superionics*, Schenectady, N.Y., pp. 1–14.

BOVIN, J.-O. (1978). *Nature (London)*, **273**, 136–138.

BRAGG, W. L., GOTTFRIED, C. & WEST, J. (1931). *Z. Kristallogr.* **77**, 255–274.

BURSILL, L. A. & WILSON, A. R. (1977). *Acta Cryst.* A**33**, 672–676.

COWLEY, J. M. & IIJIMA, S. (1972). *Z. Naturforsch. Teil A*, **27**, 445–451.

COWLEY, J. M. & MOODIE, A. F. (1957). *Acta Cryst.* **10**, 609–619.

CURIEN, H., GUILLEMIN, C., ORCEL, J. & STERNBERG, M. (1956). *C. R. Acad. Sci.* **242**, 2845–2847.

DEJONGHE, L. C. (1975). *J. Mater. Sci.* **10**, 2173–2175.

DEJONGHE, L. C. (1976). *J. Mater. Sci.* **11**, 206–208.

DEJONGHE, L. C. (1977*a*). *J. Mater. Sci.* **12**, 497–502.

DEJONGHE, L. C. (1977*b*). *Mater. Res. Bull.* **12**, 667–674.

FEJES, P. (1973). Ph.D. Thesis, Arizona State University.

GOODMAN, P. & MOODIE, A. F. (1974). *Acta Cryst.* A**30**, 280–290.

GRATIAS, D., BOILOT, J. P., LECARS, Y. & THÉRY, J. (1976). *Phys. Status Solidi A*, **38**, 595–600.

HEIDENREICH, R. D. (1964). *Fundamentals of Transmission Electron Microscopy*, p. 112. New York: Interscience.

IIJIMA, S. (1973). *Acta Cryst.* A**29**, 18–24.

LECARS, Y., GRATIAS, D., PORTIER, R. & THÉRY, J. (1975). *J. Solid State Chem.* **15**, 218–222.

O'KEEFE, M. A. (1973). *Acta Cryst.* A**29**, 389–401.

PETERS, C. R., BETTMAN, M., MOORE, J. W. & GLICK, M. D. (1971). *Acta Cryst.* B**27**, 1826–1834.

ROTH, W. L. (1972). *Proc. 5th Mater. Res. Symp. NBS Spec. Publ.* 364, pp. 129–137.

SATO, S. & HIROTSU, Y. (1976). *Mater. Res. Bull.* **11**, 1307–1318.

STEVENS, R. (1974). *J. Mater. Sci.* **9**, 801–808.

STEVENS, R. & MILES, L. J. (1976). *J. Mater. Sci.* **11**, 1911–1918.

VAN LANDUYT, J., AMELINCKX, S., KOHN, J. A. & ECKART, D. W. (1974). *J. Solid State Chem.* **9**, 103–119.

YAMAGUCHI, G. & SUZUKI, K. (1968). *Bull. Chem. Soc. Jpn*, **41**, 93–99.

Acta Cryst. (1979). A**35**, 580–583

On the Structure of Mn_5Si_3, Th_6Mn_{23} and γ-Brass

BY HARRY NYMAN AND STEN ANDERSSON

Inorganic Chemistry 2, Chemical Center, University of Lund, PO Box 740, S-220 07 Lund, Sweden

(*Received* 11 *December* 1978; *accepted* 18 *January* 1979)

Abstract

The structures of Mn_5Si_3, Th_6Mn_{23} and γ-brass are accurately derived from octahedra (Mn_5Si_3), tetrahedra and triangle-capping. The relationship between pyrochlore, Th_6Mn_{23} and γ-brass is also derived.

Introduction

Recently we showed how a unit of six triangles sharing edges with a central tetrahedron generated the essential part of a complex of four face-sharing icosahedra (Andersson, 1978). Searching for other applications of triangle-capping, we came across the structures of Mn_5Si_3, Th_6Mn_{23} and γ-brass, the latter two related to each other and also to the pyrochlore structure.

Mn_5Si_3

If the free edges of a chain of face-sharing octahedra are capped with triangles, the result is a column which can be used to construct the structure of Mn_5Si_3. Such columns put together over the free triangle corners, as shown in Fig. 1, make up the Mn framework of Mn_5Si_3. If we assume ideal triangles and octahedra, with unit edge e, cell dimensions can be derived:

$$a = e(\sqrt{3} + 3)/2; \quad c = e2\sqrt{2}/\sqrt{3}; \quad c/a = 0{\cdot}690.$$

The 6(g) parameter for the Mn atoms becomes

$$x = (\sqrt{3} - 1)/3 = 0{\cdot}244.$$

0567-7394/79/040580-05$01.00